

Article

An Ascorbic Acid-Imprinted Poly(o-phenylenediamine)/AuNPs@COF_{TFPB-NBPDA} for Electrochemical Sensing Ascorbic Acid

Yaqin Chen, Xia Peng, Yonghai Song and Guangran Ma *

National Engineering Research Center for Carbohydrate Synthesis/Key Lab of Fluorine and Silicon for Energy Materials and Chemistry of Ministry of Education, Analysis and Testing Center, College of Chemistry and Chemical Engineering, Jiangxi Normal University, 99 Ziyang Avenue, Nanchang 330022, China

* Correspondence: grma@jxnu.edu.cn; Tel./Fax: +86-791-88120861

Abstract: An electrochemical sensor based on a molecularly imprinted polymer membrane (MIP) was developed. The electrochemical sensor was prepared by electropolymerization of o-phenylenediamine (O-PD) on the surface of glassy carbon electrode (GCE), modified by AuNPs@covalent organic framework (COF) microspheres with ascorbic acid (AA) as template molecule. First, ultrasmall polyvinylpyrrolidone (PVP)-coated AuNPs were prepared by a chemical reduction method. Then, 1,3,5-tri(p-formylphenyl)benzene (TFPB) and N-boc-1,4-phenylene diamine (NBPDA) underwent an ammonaldehyde condensation reaction on PVP-coated AuNPs to form AuNPs@COF_{TFPB-NBPDA} microspheres. The porous spherical structure of AuNPs@COF_{TFPB-NBPDA} could accelerate the mass transfer, enlarge the specific surface area, and enhance the catalytic activity of PVP-coated AuNPs. The electrochemical sensors, based on AuNPs@COF_{TFPB-NBPDA}/GCE and nMIPs/AuNPs@COF_{TFPB-NBPDA}/GCE, were applied for the detection of AA, with a detection limit of 1.69 and 2.57 μM , as well as linear ranges of 5.07 to 60 mM and 7.81 to 60 mM. The nMIPs/AuNPs@COF_{TFPB-NBPDA} sensor had satisfactory stability, selectivity, and reproducibility for AA detection.

Keywords: covalent organic framework; ascorbic acid; molecularly imprinted polymer; electrochemical sensor



Citation: Chen, Y.; Peng, X.; Song, Y.; Ma, G. An Ascorbic Acid-Imprinted Poly(o-phenylenediamine)/AuNPs@COF_{TFPB-NBPDA} for Electrochemical Sensing Ascorbic Acid. *Chemosensors* **2022**, *10*, 407. <https://doi.org/10.3390/chemosensors10100407>

Academic Editors: Verónica Montes García and Alexander Castro Grijalba

Received: 17 September 2022

Accepted: 8 October 2022

Published: 10 October 2022

Publisher's Note: MDPI stays neutral with regard to jurisdictional claims in published maps and institutional affiliations.



Copyright: © 2022 by the authors. Licensee MDPI, Basel, Switzerland. This article is an open access article distributed under the terms and conditions of the Creative Commons Attribution (CC BY) license (<https://creativecommons.org/licenses/by/4.0/>).

1. Introduction

Covalent organic frameworks (COFs) are composed of organic building blocks connected by strong covalent bonds. Recently, COFs have attracted great interest, due to a series of advantages, such as unique porous crystalline structure, easy functionalization, and tunable building blocks [1–4]. However, their poor electrical conductivity and low catalysis activity limit their applications in electrocatalysis and electrochemical sensors. In order to solve the above problems, the proposed solution is to dope the metal nanoparticles into the organic framework of COFs [5–7] or change the electronic structure of the composite material; accordingly, a large number of active sites can be generated to promote the catalytic reaction. The traditional hybrid method was to complex metal precursor into the organic skeleton of COF through coordination, followed by in-situ reduction, and the metal nanoparticles are dispersed and supported on the COF. However, this template-directed approach limits the tunability of the size and shape of the metal particles [8].

Ascorbic acid (AA), commonly known as vitamin C, is a polyhydroxy compound that is widely present in fruits and vegetables [9–11]. It plays an important role in the human body and can remove the radicals produced by metabolism in the human body [12–14]. Additionally, it participates in the synthesis of various hormones and neurotransmitters in the body [15]. AA has strong antioxidant properties and can remove organic toxins in the body through auto-oxidation and reduce the rate of liver disease. In the medical field, the detection of AA in urine can rule out false negatives or positives. Therefore,

it has been widely studied in drug prevention and combination [16–18]. However, the excessive intake of AA can also lead to other diseases. For example, long-term fasting or oral intake will stimulate the gastric mucosa and damage gastrointestinal health, while long-term consumption of AA may lead to infertility in women [19]. Therefore, the accurate determination of the concentration of AA has important significance [20–22].

AA can be detected by many methods, such as fluorescence [9], chromatography [23], and ultraviolet detection [24], but the electrochemical methods offer the advantages of high sensitivity, accuracy, low cost, ease of use, and portability of equipment [25–31]. Up until now, many researchers have reported a series of related works. For example, Jiang et al. fabricated a facile ratiometric electrochemical sensor for the online measurement of AA in brain micro dialysates in vivo [32]. Wang et al. constructed a ratiometric electrochemical AA sensor by growing electroactive COF on the surface of multi-walled carbon nanotubes and modifying the composites onto a glassy carbon electrode (GCE) [33]. Ma et al. loaded PtNPs on the GCE surface by electrodeposition method, and then deposited a layer of zeolite imidazolate framework material (ZIF-8) film on the surface for the detection of AA [34]. The molecular imprinting technology combines molecularly imprinted polymers (nMIPs) with electrochemical sensors to simulate antigen-antibody complexes in organisms, so as to improve the selectivity of the electrochemical sensors [35–37]. The essential idea is to use the detected molecules as templates to form MIPs with relevant functional monomers, through covalent or non-covalent bonds. After eluting and removing the detected molecules, nMIPs with a particular identification ability and high stability can be obtained [38–40].

Therefore, in this work, a MIP-based electrochemical sensor for the detection of AA was designed. Ultrasmall polyvinylpyrrolidone (PVP)-coated AuNPs were firstly prepared. Then, COF_{TFPB-NBPDA} was grown on PVP-coated AuNPs by amine-aldehyde condensation reaction between 1,3,5-tri(p-formylphenyl)benzene (TFPB) and N-boc-1,4-phenylene diamine (NBPDA) to prepare the AuNPs@COF_{TFPB-NBPDA} microspheres. The porous spherical structure of AuNPs@COF_{TFPB-NBPDA} can accelerate the mass transfer, enlarge the specific surface area, and enhance the catalytic activity of PVP-coated AuNPs. The AuNPs@COF_{TFPB-NBPDA} also has good electrical conductivity and catalytic activity; accordingly, the AuNPs@COF_{TFPB-NBPDA} directly catalyzes the oxidation reaction of AA. Finally, an electrochemical sensor based on nMIPs/AuNPs@COF_{TFPB-NBPDA}/GCE was prepared by electropolymerization of o-phenylenediamine (O-PD) on the surface of GCE modified by AuNPs@COF_{TFPB-NBPDA} microspheres, with AA as the template molecule. The electrochemical sensor based on nMIPs/AuNPs@COF_{TFPB-NBPDA}/GCE was applied for the detection of AA, showing satisfactory performances.

2. Experimental

2.1. Reagents

The 1,3,5-tris(p-formylphenyl)benzene (TFPB) and N-boc-1,4-phenylene diamine (NBPDA) were obtained from Yanshen Technology Co., Ltd. (Jilin, China). Trifluoroacetic acid (TFA), triethylamine, and ethanol were purchased from Inoke Technology Co., Ltd. (Beijing, China). Chloroauric acid, glucose, uric acid, ascorbic acid (AA), o-phenylenediamine (O-PD), acetic acid (HAc), sodium acetate (NaAc), NaCl, and KCl are supplied from Aladdin Reagent Network. Glassy carbon electrode (GCE) was purchased from Chenhua Instrument Co., Ltd. (Shanghai, China). Effervescent tablets were purchased from Yabao Pharmaceutical Group Co., Ltd. (Shanxi, China). The 0.2 M phosphate buffered solution was prepared from 0.2 M sodium dihydrogen phosphate and disodium hydrogen phosphate solutions in different proportions. Acetic acid buffer solution with pH = 5.2 was prepared by mixing 0.2 mol/L HAc solution with 0.2 mol/L NaAc solution, at a volume ratio of 2.1:7.9. The ultrapure water used in the experiment was purified by Millipore-Q System ($\rho \geq 18.2 \text{ M}\Omega \text{ cm}$).

2.2. Instruments

Transmission electron microscopy (TEM) images were acquired using JEM-2010 (HR) (Japan Electronics Co., Ltd., Tokyo, Japan). Scanning electron microscopy (SEM) images were collected by using HITACHI S-3400N instrument (Hitachi Limited, Tokyo, Japan), and the breakdown voltage was set to 15 kV. X-ray powder diffraction (XRD) analysis was performed using a D/Max 2500 V/PC (Rigaku Corporation, Tokyo, Japan) instrument, with Cu K α radiation from 2° to 35°, at a scanning rate of 1°/min. Fourier transform infrared spectroscopy (FTIR) was obtained on a spectrometer model Perkin-Elmer Spectromer 100 (Perkin-Elmer, Waltham, MA, USA). N₂ adsorption/desorption isotherm tests were carried out by Autosorb-iQ (Quantachrome, Boynton Beach, FL, USA) under 77 K. All electrochemical studies were performed on an electrochemical workstation, model CHI 760D (Chenhua Instrument Co., Ltd., Shanghai, China). A conventional three-electrode system was used, where the reference electrode was a saturated calomel electrode (SCE), the counter electrode was a platinum wire electrode, and the working electrodes were different modified electrodes. Cyclic voltammetry (CVs) and electrochemical impedance spectroscopy (EIS) were performed in 0.1 M KCl solution containing 5.0 mM [Fe(CN)₆]^{3−/4−} at frequencies ranging from 0.01 to 100 KHz and open circuit voltages. AC impedance is used to analyze the electron transport rate and interface state of ion transport at various stages. Differential pulse voltammetry (DPV) tests were performed in 0.2 M static phosphate buffered solution (pH = 7.0).

2.3. Synthesis of AuNPs@COF_{TFPB-NBPDA}

The HAuCl₄ solution (50 mL, 10 mM) was added in a 250 mL round-bottom flask under stirring. Then, the round-bottom flask was heated. When the temperature reached 60 °C, trisodium citrate solution (2 mL, 200 mM) was added. It was observed that, after 1 min, the solution changed from yellow to red. Heating was stopped after stirring for 10 min, and the solution was cooled down to room temperature. Then, 10 mg PVP was added into 10 mL AuNPs solution to obtain PVP-coated AuNPs. The schematic diagram of the preparation process of PVP-coated AuNPs was shown in Figure 1a.

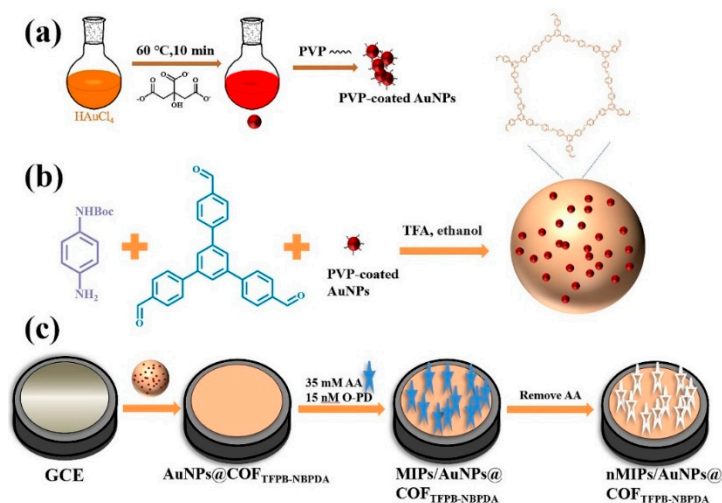


Figure 1. Schematic diagram of the preparation process of (a) PVP-coated AuNPs, (b) AuNPs@COF_{TFPB-NBPDA}, and (c) nMIP/AuNPs@COF_{TFPB-NBPDA}/GCE.

The COF_{TFPB-NBPDA} was prepared according to the solvothermal synthesis method. The 0.06 mM TFPB and 0.1 mmol NBPDA were dissolved in 2 mL of ethanol. After the solution was completely dissolved, 240 μ L TFA was added, and the reaction was carried out in a 120 °C oven for 12 h. The resulting pellet was diluted to 10 mL with ethanol and centrifuged at 10000 r.p.m. for 10 min in a centrifuge. A total of 500 μ L of triethylamine was added to the above solution, and the solution changed from red to yellow. The product

(COF_{TFPB-NBPDA}) was then washed with ethanol several times, until the supernatant was clear. The procedure to prepare AuNPs@COF_{TFPB-NBPDA} was similar to the preparation of COF_{TFPB-NBPDA}. After 0.06 mM TFPB and 0.1 mmol NBPDA were dissolved in 2 mL of ethanol, the 500 μ L of the AuNPs solution was added. The subsequent steps were the same as above. The schematic diagram of the preparation process of AuNPs@COF_{TFPB-NBPDA} is shown in Figure 1b.

2.4. Preparation of nMIP/AuNPs@COF_{TFPB-NBPDA} and NIP/AuNPs@COF_{TFPB-NBPDA}

A total of 5 μ L 2 mg mL⁻¹ AuNPs@COF_{TFPB-NBPDA} was dropped on the polished GCE to obtain AuNPs@COF_{TFPB-NBPDA}/GCE. Then, 0.0162 g of O-PD and 0.0528 g of AA were dissolved in 10 mL acetic acid buffer solution (pH = 5.2). A high template concentration is required for obtaining more imprinted holes. Then, electrodeposition was carried out in the above solution by cyclic voltammetry, at a potential of 0–0.8 V for 20 cycles, in order to obtain MIP/AuNPs@COF_{TFPB-NBPDA}/GCE. The NIP/AuNPs@COF_{TFPB-NBPDA}/GCE was prepared in the same way as MIP/AuNPs@COF_{TFPB-NBPDA}/GCE, except that AA was not added to the solution. The model electroactive molecule AA was eluted by soaking MIP/AuNPs@COF_{TFPB-NBPDA}/GCE in ultrapure water for 30 min to obtain the nMIP/AuNPs@COF_{TFPB-NBPDA}/GCE. The preparation process of nMIP/AuNPs@COF_{TFPB-NBPDA}/GCE is shown in the Figure 1c.

2.5. Preparation of Real Samples

Vitamin C tablets (100 mg/tablet) were ground in an agate mortar and weighed, and 1/20 of them was dissolved in 10 mL phosphate buffered solution (pH = 6.5) as the mother liquor of real samples.

3. Results and Discussion

3.1. Characterization of COF_{TFPB-NBPDA} and AuNPs@COF_{TFPB-NBPDA}

SEM images of COF_{TFPB-NBPDA} showed that the COF_{TFPB-NBPDA} exists in spherical form, with a diameter of about 2–3 μ m (Figure S1). Next, the COF_{TFPB-NBPDA} was investigated by FT-IR spectra (Figure S2a). Compared with TFPB and NBPDA, the COF_{TFPB-NBPDA} had a new peak at 1675 cm⁻¹, which belonged to the C=N stretching vibration peak formed by amino aldehyde condensation. This result proves the successful synthesis of COF_{TFPB-NBPDA}. XRD was used to study the crystallinity of the synthesized COF_{TFPB-NBPDA} material. Figure S2b shows that a high-intensity diffraction peak of COF_{TFPB-NBPDA} appeared in the low-angle region of $2\theta = 2.72^\circ$, which belongs to the (100) crystal plane. In addition, there was a broad and weak peak at $2\theta = 19.95^\circ$ in the XRD, which belongs to the (001) crystal plane. The above results confirm that the COF_{TFPB-NBPDA} material has good crystallinity. Figure S2c is the N₂ isotherm adsorption and desorption curve of the material. It can be seen that the specific surface area of the COF_{TFPB-NBPDA} materials was about 66.09 m² g⁻¹, which may be due to the accumulation of COF_{TFPB-NBPDA}. Figure S2d shows that the pore size of COF_{TFPB-NBPDA} was around 3 nm.

The morphology of the AuNPs@COF_{TFPB-NBPDA} was investigated by TEM. Up until now, many researchers have synthesized a series of nano-gold materials, such as AuNPs, gold nanorods, and gold nanoclusters, and most of them have uniform morphologies [41–43]. However, in order to expose more active sites of AuNPs and improve the catalytic effect of the material, a large number of small-sized AuNPs were prepared here by the chemical reduction method (Figure 2a). Figure 2b shows that the resulting AuNPs were about 7 nm in diameter and had good crystallinity. From the TEM images, the AuNPs@COF_{TFPB-NBPDA} was observed to be clustered, and the clusters were superimposed by many two-dimensional sheets (Figure 2c). The diameters of these clusters were about 200 nm, and a large number of small-sized AuNPs were distributed inside them, which were prepared in the previous step (Figure 2d). After the AuNPs were functionalized with PVP, there was many -NH₂ on the AuNPs surface that could be covalently bound to COF_{TFPB-NBPDA}. With the addition of monomers, the -CHO of TPBA reacted with -NH₂ to

produce $\text{COF}_{\text{TFPB-NBPDA}}$, with AuNPs as the core and two-dimensional flakes growing on the outer shell.

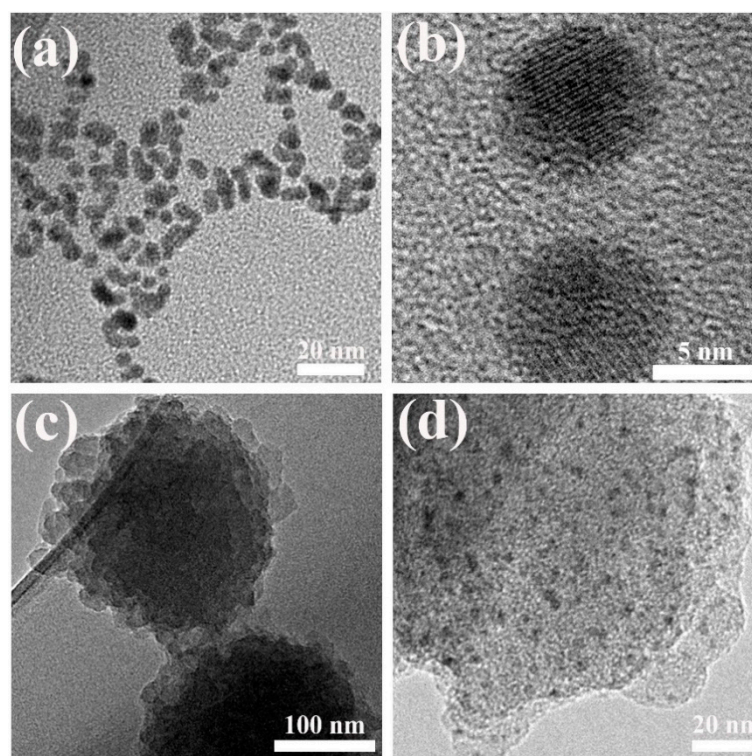


Figure 2. (a,b) TEM images of AuNPs under different magnification; (c,d) TEM images of AuNPs@ $\text{COF}_{\text{TFPB-NBPDA}}$ under different magnification.

3.2. Electrochemical Behaviors of $\text{COF}_{\text{TFPB-NBPDA}}/\text{GCE}$ and $\text{AuNPs}@ \text{COF}_{\text{TFPB-NBPDA}}/\text{GCE}$

The electrochemical performance of $\text{AuNPs}@ \text{COF}_{\text{TFPB-NBPDA}}/\text{GCE}$ was evaluated by CV and EIS, and the inset in Figure 3b shows the equivalent circuit diagram. Figure 3a shows the CVs of GCE, $\text{COF}_{\text{TFPB-NBPDA}}/\text{GCE}$, and $\text{AuNPs}@ \text{COF}_{\text{TFPB-NBPDA}}/\text{GCE}$ in the 0.1 M KCl and 5.0 mM $\text{Fe}[(\text{CN})_6]^{3-/4-}$ solution. It can be seen that, after the modification of $\text{COF}_{\text{TFPB-NBPDA}}$ or $\text{AuNPs}@ \text{COF}_{\text{TFPB-NBPDA}}$ on the GCE surface, the peak-to-peak potential difference of the modified electrodes increased from 0.08 to 0.095 or 0.090 V, while its peak current decreased, instead. In contrast, $\text{AuNPs}@ \text{COF}_{\text{TFPB-NBPDA}}/\text{GCE}$ showed similar electrochemical properties to bare GCE, thus proving that the as-prepared $\text{AuNPs}@ \text{COF}_{\text{TFPB-NBPDA}}$ had good electrical conductivity.

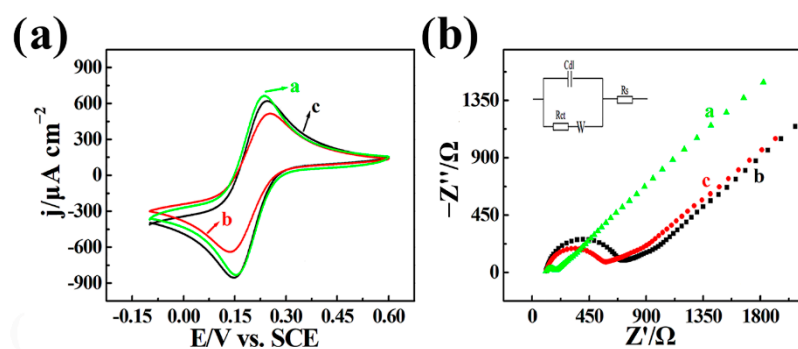


Figure 3. (a) CVs and (b) EIS (inset: equivalent circuit diagram) of GCE (curve a, green line), $\text{COF}_{\text{TFPB-NBPDA}}/\text{GCE}$ (curve b, red line), and $\text{AuNPs}@ \text{COF}_{\text{TFPB-NBPDA}}/\text{GCE}$ (curve c, black line) in 0.1 M KCl solution containing 5 mM $\text{Fe}[(\text{CN})_6]^{3-/4-}$ probe.

Compared with bare GCE, the resistance of the modified $\text{COF}_{\text{TFPB-NBPDA}}/\text{GCE}$ was significantly increased, about 500Ω (Figure 3b). The reason for this result might be the existence of interlayer π - π interaction in 2D organic framework materials, which hindered the electron transport. However, when $\text{AuNPs}@ \text{COF}_{\text{TFPB-NBPDA}}$ was modified on the surface of GCE, AuNPs enhanced the conductivity of the bulk material, thus resulting in the decrease in its resistance value. These results are consistent with that shown in Figure 3a, indicating that the as-prepared $\text{AuNPs}@ \text{COF}_{\text{TFPB-NBPDA}}$ can enhance the electron transport of the electrode, which is beneficial to the electrochemical sensor.

3.3. Electrochemical Detection of AA by $\text{AuNPs}@ \text{COF}_{\text{TFPB-NBPDA}}/\text{GCE}$ and $n\text{MIPs}/\text{AuNPs}@ \text{COF}_{\text{TFPB-NBPDA}}/\text{GCE}$

The preparation of $\text{AuNPs}@ \text{COF}_{\text{TFPB-NBPDA}}/\text{GCE}$ and its use in AA detection are susceptible to many factors, including the pH of the electrolyte solution, the volume of the AuNPs solution during the preparation process, and the volume of the $\text{AuNPs}@ \text{COF}_{\text{TFPB-NBPDA}}$ dispersion on the electrode surface. In order to obtain the optimum detection effect, the above three parameters were optimized. First of all, the electrochemical responses of the electrodes in different pH electrolyte solutions under the same conditions were investigated by DPV, and the electrolyte solutions were prepared from Na_2HPO_4 (0.2 M) and NaH_2PO_4 (0.2 M) solutions. As can be seen from Figure S3a, with the increase of pH, the oxidation peak current of AA showed a trend of firstly increasing and then decreasing. When pH = 6.5, the electrochemical response value reached the maximum, thus pH = 6.5 was adopted as the optimal condition for subsequent detection. As shown in Figure S4, the peak current of AA slightly increased as the pH increased from 6 to 6.5, accompanied by the peak potential negatively shifted. With the increase of pH from 6.5 to 7.5, the peak current decreased and peak potential almost unchanged.

Then the electrocatalytic performance of $\text{AuNPs}@ \text{COF}_{\text{TFPB-NBPDA}}/\text{GCE}$ constructed by $\text{AuNPs}@ \text{COF}_{\text{TFPB-NBPDA}}$ prepared with different volumes of AuNPs solution was explored, and the results are shown in Figure S3b. The volume of AuNPs solution was changed while TFPB was maintained as 0.06 mmol and NBPDA was maintained as 0.1 mmol. When the volume of AuNPs solution was increased from 250 μL to 500 μL , the response value of AA increased significantly and reached a peak value. The reason can be attributed to with the increase of the volume of AuNPs solution, the active sites in the $\text{AuNPs}@ \text{COF}_{\text{TFPB-NBPDA}}$ material also increased, and the enrichment of AA on its surface achieved the best catalytic effect. While the volume was further increased from 500 μL to 1000 μL , the response value decreased instead. Perhaps excessive AuNPs would lead to the aggregation of the target material and cause the decrease of the catalytic effect of $\text{AuNPs}@ \text{COF}_{\text{TFPB-NBPDA}}/\text{GCE}$. Therefore, 500 μL of AuNPs was chosen as the optimal volume for the preparation of $\text{AuNPs}@ \text{COF}_{\text{TFPB-NBPDA}}$.

Next, the modification amount of $\text{AuNPs}@ \text{COF}_{\text{TFPB-NBPDA}}$ on the electrode surface was optimized. 2 mg mL^{-1} $\text{AuNPs}@ \text{COF}_{\text{TFPB-NBPDA}}$ solution was prepared, and different volume of 2.5 μL , 5.0 μL , 7.5 μL and 10.0 μL were modified to the electrode surface, respectively. The results are shown in Figure S3c. With the increase of modification volume, the peak current density of AA on the $\text{AuNPs}@ \text{COF}_{\text{TFPB-NBPDA}}/\text{GCE}$ increased first and then decreased, and reached the maximum at 5.0 μL . The reason may be that the catalytic sites gradually increased as the $\text{AuNPs}@ \text{COF}_{\text{TFPB-NBPDA}}$ material increased at first, the current response increased accordingly. After reaching the maximum loading, $\text{AuNPs}@ \text{COF}_{\text{TFPB-NBPDA}}$ material would accumulate on the electrode surface, and the modified layer became thicker, which hindered the electron transport and reduced the catalytic effect of $\text{AuNPs}@ \text{COF}_{\text{TFPB-NBPDA}}/\text{GCE}$. Therefore, 5.0 μL was chosen as the optimal modification amount for the assay.

In order to test the electrocatalytic performance of the prepared materials, different modified electrodes including GCE, $\text{COF}_{\text{TFPB-NBPDA}}/\text{GCE}$ s and $\text{AuNPs}@ \text{COF}_{\text{TFPB-NBPDA}}/\text{GCE}$ were prepared and used to detect AA by DPV in 0.2 M phosphate buffered solution (pH = 6.5) (Figure 4a). After the addition of 30 mM AA, the loaded $\text{COF}_{\text{TFPB-NBPDA}}$ ma-

material showed higher peak current density values, and the peak potential also negatively shifted slightly. This indicated that the prepared $\text{COF}_{\text{TFPB-NBPDA}}$ had certain catalytic activity and could catalyze the oxidation of AA. However, after $\text{AuNPs}@COF_{\text{TFPB-NBPDA}}$ was modified on the electrode surface, the peak current response value was further increased, and the peak potential was further negatively shifted. This proved that the $\text{AuNPs}@COF_{\text{TFPB-NBPDA}}$ has better catalytic activity toward AA. The high electrical conductivity of $\text{AuNPs}@COF_{\text{TFPB-NBPDA}}$ accelerated the electron transfer to AA during oxidation process, and the rich aromatic system in $\text{COF}_{\text{TFPB-NBPDA}}$ facilitated π - π stacking interactions with AA. Furthermore, the large surface area of $\text{AuNPs}@COF_{\text{TFPB-NBPDA}}$ provided abundant sites for AA binding. Due to the existence of AuNPs, the overpotential of the oxidation was reduced, making AA easier to be oxidized, so the more negative the oxidation potential was shifted negatively.

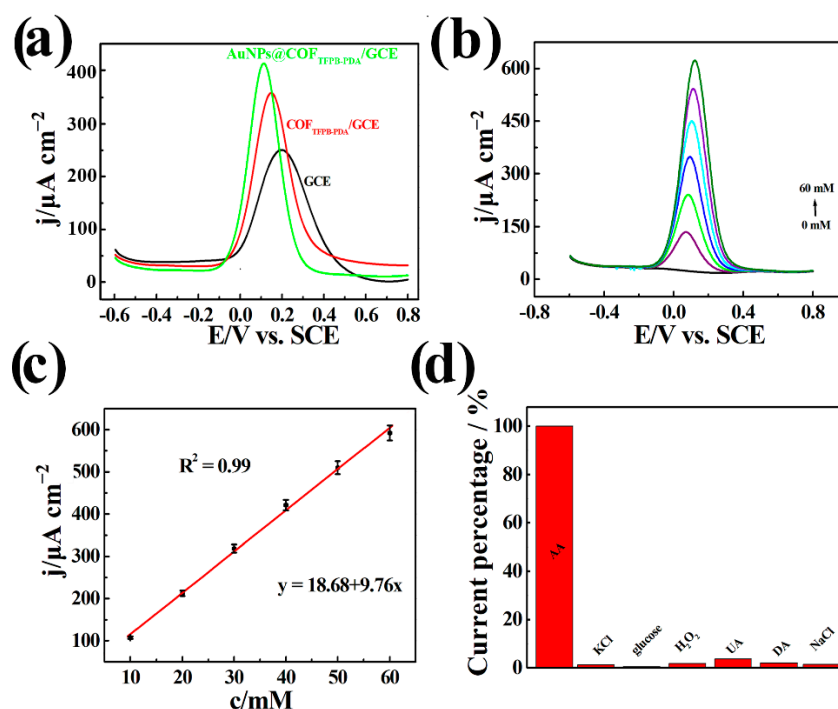


Figure 4. (a) DPV of GCE, $\text{COF}_{\text{TFPB-NBPDA}}/\text{GCE}$ and $\text{AuNPs}@COF_{\text{TFPB-NBPDA}}/\text{GCE}$ in 0.2 M phosphate buffered solution (pH = 6.5) with 30 mM AA; (b) DPV of $\text{AuNPs}@COF_{\text{TFPB-NBPDA}}/\text{GCE}$ AA in 0.2 M phosphate buffered solution (pH = 6.5) with different concentration of AA; (c) The corresponding linear relationship between peak current density and the concentration of AA; (d) The diagram of $\text{AuNPs}@COF_{\text{TFPB-NBPDA}}/\text{GCE}$ to different interfering substances.

Under these optimal conditions, the electrochemical sensor based on the $\text{AuNPs}@COF_{\text{TFPB-NBPDA}}/\text{GCE}$ was used to detect AA, and the specific results are shown in Figure 4b. With the addition of different concentration of AA, the peak current density value of the $\text{AuNPs}@COF_{\text{TFPB-NBPDA}}/\text{GCE}$ increased accordingly, and the correlation reaches 0.99, indicating a good linear correlation (Figure 4c). In addition, the peak potential of AA also gradually positively shifted with the increase of its concentration, which might be due to the accumulation of the oxidation products of AA on the electrode surface. The constructed $\text{AuNPs}@COF_{\text{TFPB-NBPDA}}/\text{GCE}$ had a linear range of 5.07 μM –60 mM, and its detection limit was 1.69 μM . In addition, the selectivity was also an important factor in evaluating the performance of the sensor. Different interfering substances was added into the solution of 30 mM AA, including dopamine, uric acid and glucose, etc. The variation was only 3.7%, indicating that the proposed sensor had acceptable selectivity for standard samples (Figure 4d).

Then, the electrochemical performance of nMIP/AuNPs@COF_{TFPB-NBPDA} was studied. The AA-O-PD molecularly imprinted membrane (MIP) was electropolymerized to the AuNPs@COF_{TFPB-NBPDA} surface using cyclic voltammetry to improve the selectivity and stability of electrochemical sensors. As illustrated in Figure 5a, the area of CVs curve diminished gradually, which implied that the MIP was gradually electropolymerized on the AuNPs@COF_{TFPB-NBPDA}/GCE surface. The area of CV curves approached zero due to the weak conductivity of MIP [44]. The encapsulation of AA in MIP was confirmed by Figure S5, in which an obvious oxidation peak of AA appeared. As a comparison, in the absence of AA, NIP/AuNPs@COF_{TFPB-NBPDA}/GCE did not show oxidation peak (Figure S6). This could be the extremely poor conductivity of the Po-PD polymeric film, which led to the inability transport and transfer of electron. The AA model electroactive molecules were eluted to form nMIP/AuNPs@COF_{TFPB-NBPDA}/GCE. Then, the nMIP/AuNPs@COF_{TFPB-NBPDA}/GCE was utilized to detect AA, and the results was showed in Figure 5b. The peak current density increased accordingly as different concentrations of AA were added, and the correlation reached 0.99, demonstrating high linear correlation (Figure 5c). The nMIP/AuNPs@COF_{TFPB-NBPDA}/GCE was applied for the detection of AA as an electrochemical sensor with a linear range of 7.81 μM to 60 mM and a detection limit as low as 2.57 μM . In addition, the selectivity was also assessed. The interferences were the same as those of AuNPs@COF_{TFPB-NBPDA}/GCE. The variation was only 2.6% indicating that the proposed sensor had acceptable selectivity (Figure 5d). Compared with other electrochemical sensors, the nMIP/AuNPs@COF_{TFPB-NBPDA}/GCE sensor has certain advantages (Table S1) [34,45–53]. Compared with NOCC-O, S-fs-ERG, ZIF-8/PtNPs/GCE, ZnHCFSSQ-H/GPE and MVCMM materials, the prepared nMIP/AuNPs@COF_{TFPB-NBPDA} had lower detection limit; while compared with Ni₃(HITP)₂/SPCE, film-1/ITO, rGO-AuNPs, GO/NNO₁₀₀, and CuO, the nMIP/AuNPs@COF_{TFPB-NBPDA}/GCE had a wider detection range.

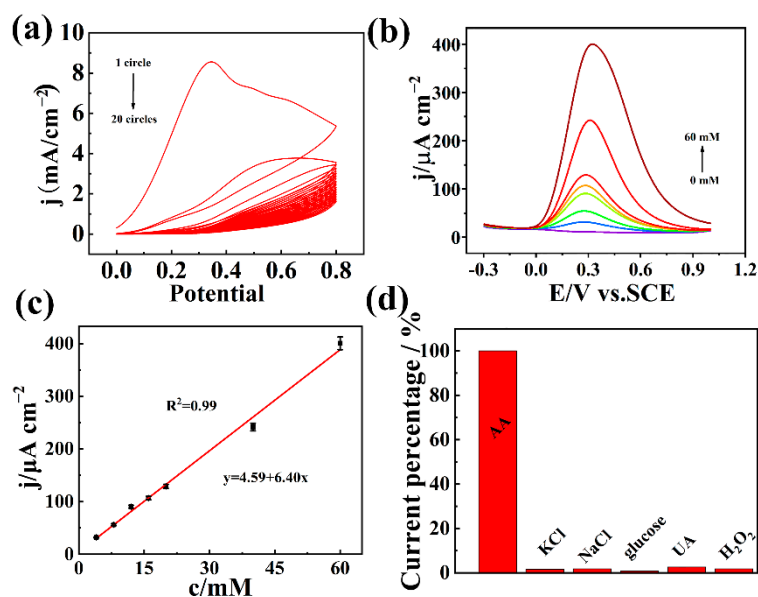


Figure 5. (a) CVs of nMIP/AuNPs@COF_{TFPB-NBPDA} during electropolymerization; (b) DPV of AA detected by nMIP/AuNPs@COF_{TFPB-NBPDA}/GCE; (c) Linear relationship between response current of nMIP/AuNPs@COF_{TFPB-NBPDA}/GCE and AA concentration; (d) Diagram of nMIP/AuNPs@COF_{TFPB-NBPDA}/GCE to different interfering substances.

3.4. Detection of AA in Effervescent Tablets

To test the feasibility of the sensor in practical applications, a nMIP/AuNPs@COF_{TFPB-NBPDA}/GCE sensor was used to detect AA in effervescent tablets. The standard addition method was used. The results are shown in Table S2. It can be seen that the recov-

eries of three different concentrations of AA were in the range of 99–101%, and the RSD of those results were less than 7%. The result show that nMIP/AuNPs@COF_{TFPB-NBPDA}/GCE had the potential for the detection of real sample.

4. Conclusions

In conclusion, ultrasmall-sized, PVP-capped AuNPs were synthesized first, and then AuNPs@COF_{TFPB-NBPDA} was prepared by one-pot method. The AuNPs@COF_{TFPB-NBPDA} is a nanosphere with a diameter of about 200 nm, and there are numerous two-dimensional nanosheets on its surface. The abundant functional groups and well-ordered pores of COF_{TFPB-NBPDA} caused the AuNPs to be uniformly loaded on the COF_{TFPB-NBPDA}, and the good electrical conductivity and catalytic activity of AuNPs improved the catalytic effect of the AA oxidation. The obtained AuNPs@COF_{TFPB-NBPDA} composite had smaller size and better catalytic activity than COF_{TFPB-NBPDA}. Additionally, an electrochemical sensor based on nMIP/AuNPs@COF_{TFPB-NBPDA} was designed using AA as a model electroactive molecule and O-PD as a functional monomer for the selective detection of AA. Anyway, the proposed nMIP/AuNPs@COF_{TFPB-NBPDA}/GCE electrochemical sensor had good selectivity and stability.

Supplementary Materials: The following supporting information can be downloaded at: <https://www.mdpi.com/article/10.3390/chemosensors10100407/s1>. Figure S1: SEM images of COF_{TFPB-NBPDA}. Figure S2: (a) FT-IR spectra of COF_{TFPB-NBPDA}, TFPB, and NBPDA. (b) Wide-angle XRD pattern of COF_{TFPB-NBPDA}. (c) N₂ adsorption-desorption isotherm of COF_{TFPB-NBPDA}. (d) COF_{TFPB-NBPDA} pore size distributions. Figure S3. Effects of (a) pH of electrolyte solution, (b) volume of AuNPs solution, and (c) volume of AuNPs@COF_{TFPB-NBPDA} dispersion on electrode surface on the peak current density of AuNPs@COF_{TFPB-NBPDA}/GCE for detection of AA. Figure S4: DPV of AuNPs@COF_{TFPB-NBPDA}/GCE in 0.2 M phosphate buffered solution different pH in the presence of 30 mM AA. Figure S5: DPV of MIP/AuNPs@COF_{TFPB-NBPDA}/GCE in 0.2 M phosphate buffered solution (pH = 6.5). Figure S6: CVs of NIP/AuNPs@COF_{TFPB-NBPDA}/GCE in 5 mM K₃[Fe(CN)₆] with 0.1 M KCl. Table S1: Performance comparison of different AA electrochemical sensors. Table S2: Detection of AA in effervescent tablets by nMIP/AuNPs@COF_{TFPB-NBPDA}/GCE in 0.2 M phosphate buffered solution (pH = 6.5).

Author Contributions: Conceptualization, Y.S.; methodology, X.P.; validation, X.P. and Y.C.; formal analysis, Y.C. and X.P.; investigation, Y.C.; resources, G.M.; writing—original draft preparation, Y.C.; writing—review and editing, Y.S.; supervision, Y.S. and G.M.; project administration G.M.; funding acquisition, Y.S. All authors have read and agreed to the published version of the manuscript.

Funding: This work was financially supported by the National Natural Science Foundation of China (21964010).

Institutional Review Board Statement: Not applicable.

Informed Consent Statement: Not applicable.

Data Availability Statement: The data is available under the request to the correspondence.

Conflicts of Interest: The authors declare no competing financial interest.

References

1. Han, J.; Yu, J.; Guo, Y.; Wang, L.; Song, Y. COF_{BTL-1}/three-dimensional macroporous carbon electrode for simultaneous electrochemical detection of Cd²⁺, Pb²⁺, Cu²⁺ and Hg²⁺. *Sens. Actuators B-Chem.* **2020**, *321*, 128498. [CrossRef]
2. Liang, H.; Luo, Y.; Li, Y.; Song, Y.; Wang, L. An Immunosensor Using Electroactive COF as Signal Probe for Electrochemical Detection of Carcinoembryonic Antigen. *Anal. Chem.* **2022**, *94*, 5352–5358. [CrossRef] [PubMed]
3. Wang, L.; Yang, Y.; Liang, H.; Wu, N.; Peng, X.; Wang, L.; Song, Y. A novel N,S-rich COF and its derived hollow N,S-doped carbon@Pd nanorods for electrochemical detection of Hg²⁺ and paracetamol. *J. Hazard. Mater.* **2021**, *409*, 124528. [CrossRef] [PubMed]
4. Wu, N.; Wang, L.; Xie, Y.; Du, Y.; Song, Y.; Wang, L. Double signal ratiometric electrochemical riboflavin sensor based on macroporous carbon/electroactive thionine-contained covalent organic framework. *J. Colloid Interface Sci.* **2022**, *608*, 219–226. [CrossRef] [PubMed]

5. Rodriguez-San-Miguel, D.; Yazdi, A.; Guillerm, V.; Perez-Carvajal, J.; Puentes, V.; MasPOCH, D.; Zamora, F. Confining Functional Nanoparticles into Colloidal Imine-Based COF Spheres by a Sequential Encapsulation-Crystallization Method. *Chem.–A Eur. Journal*. **2017**, *23*, 8623–8627. [[CrossRef](#)] [[PubMed](#)]
6. Xu, Y.; Shi, X.; Hua, R.; Zhang, R.; Yao, Y.; Zhao, B.; Liu, T.; Zheng, J.; Lu, G. Remarkably catalytic activity in reduction of 4-nitrophenol and methylene blue by Fe₃O₄@COF supported noble metal nanoparticles. *Appl. Catal. B-Environ.* **2020**, *260*, 118142. [[CrossRef](#)]
7. Zhu, Q.-Q.; Zhang, W.-W.; Zhang, H.-W.; Yuan, R.; He, H. Elaborately manufacturing an electrochemical aptasensor based on gold nanoparticle/COF composites for amplified detection performance. *J. Mater. Chem. C* **2020**, *8*, 16984–16991. [[CrossRef](#)]
8. Guntern, Y.T.; Vavra, J.; Karve, V.V.; Varandili, S.B.; Lecina, O.S.; Gadiyar, C.; Buonsanti, R. Synthetic Tunability of Colloidal Covalent Organic Framework/Nanocrystal Hybrids. *Chem. Mater.* **2021**, *33*, 2646–2654. [[CrossRef](#)]
9. Kong, Y.; He, Y.; Zhou, J.; Zhong, S.; Song, G. Amino Acids as the Nitrogen Source to Synthesize Boron Nitride Quantum Dots for Fluorescence Turn-off-on Detection of Ascorbic Acid. *Chemistryselect* **2020**, *5*, 3828–3834. [[CrossRef](#)]
10. Yan, X.; He, L.; Zhou, C.; Qian, Z.-J.; Hong, P.; Sun, S.; Li, C. Fluorescent detection of ascorbic acid using glutathione stabilized Au nanoclusters. *Chem. Phys.* **2019**, *522*, 211–213. [[CrossRef](#)]
11. Zhang, Y.; Xiao, Y.T.; Zhang, Y.J.; Wang, Y.T. Carbon Quantum Dots as Fluorescence Turn-Off-On Probe for Detecting Fe³⁺ and Ascorbic Acid. *J. Nanosci. Nanotechnol.* **2020**, *20*, 3340–3347. [[CrossRef](#)] [[PubMed](#)]
12. Liu, J.; Pu, H.; Chen, C.; Liu, Y.; Bai, R.; Kan, J.; Jin, C. Reaction Mechanisms and Structural and Physicochemical Properties of Caffeic Acid Grafted Chitosan Synthesized in Ascorbic Acid and Hydroxyl Peroxide Redox System. *J. Agric. Food Chem.* **2018**, *66*, 279–289. [[CrossRef](#)] [[PubMed](#)]
13. Mou, J.; Wang, C.; Li, Q.; Qi, X.; Yang, J. Preparation and antioxidant properties of low molecular holothurian glycosaminoglycans by H₂O₂/ascorbic acid degradation. *Int. J. Biol. Macromol.* **2018**, *107*, 1339–1347. [[CrossRef](#)] [[PubMed](#)]
14. Njus, D.; Kelley, P.M.; Tu, Y.-J.; Schlegel, H.B. Ascorbic acid: The chemistry underlying its antioxidant properties. *Free. Radic. Biol. Med.* **2020**, *159*, 37–43. [[CrossRef](#)]
15. Qu, C.L.; Li, H.; Zhou, S.; Li, G.D.; Wang, C.; Snyders, R.; Bittencourt, C.; Li, W.J. Bi₂S₃/rGO Composite Based Electrochemical Sensor for Ascorbic Acid Detection. *Chemosensors* **2021**, *9*, 190. [[CrossRef](#)]
16. Kosuru, R.Y.; Roy, A.; Bera, S. Antagonistic Roles of Gallates and Ascorbic Acid in Pyomelanin Biosynthesis of *Pseudomonas aeruginosa* Biofilms. *Curr. Microbiol.* **2021**, *78*, 3843–3852. [[CrossRef](#)]
17. Kwiecinska-Pirog, J.; Skowron, K.; Bogiel, T.; Bialucha, A.; Przekwas, J.; Gospodarek-Komkowska, E. Vitamin C in the Presence of Sub-Inhibitory Concentration of Aminoglycosides and Fluoroquinolones Alters *Proteus mirabilis* Biofilm Inhibitory Rate. *Antibiotics* **2019**, *8*, 116. [[CrossRef](#)]
18. Patel, P.; Parmar, K.; Patel, D.; Kumar, S.; Trivedi, M.; Das, M. Inhibition of amyloid fibril formation of lysozyme by ascorbic acid and a probable mechanism of action. *Int. J. Biol. Macromol.* **2018**, *114*, 666–678. [[CrossRef](#)]
19. Tortolini, C.; Tasca, F.; Venneri, M.A.; Marchese, C.; Antiochia, R. Gold Nanoparticles/Carbon Nanotubes and Gold Nanoporous as Novel Electrochemical Platforms for L-Ascorbic Acid Detection: Comparative Performance and Application. *Chemosensors* **2021**, *9*, 229. [[CrossRef](#)]
20. Chen, H.; Liu, Y.; Li, H.; Zhang, Y.; Yao, S. Non-oxidation reduction strategy for highly selective detection of ascorbic acid with dual-ratio fluorescence and colorimetric signals. *Sens. Actuators B-Chem.* **2019**, *281*, 983–988. [[CrossRef](#)]
21. He, W.; Liu, R.; Zhou, P.; Liu, Q.; Cui, T. Flexible micro-sensors with self-assembled graphene on a polyolefin substrate for dopamine detection. *Biosens. Bioelectron.* **2020**, *167*, 112473. [[CrossRef](#)]
22. Sequeira, I.R. Higher doses of ascorbic acid may have the potential to promote nutrient delivery via intestinal paracellular absorption. *World J. Gastroenterol.* **2021**, *27*, 6750–6756. [[CrossRef](#)] [[PubMed](#)]
23. Turak, F.; Güzel, R.; Dinç, E. Simultaneous determination of ascorbic acid and caffeine in commercial soft drinks using reversed-phase ultraperformance liquid chromatography. *J. Food Drug. Anal.* **2017**, *25*, 285–292. [[CrossRef](#)] [[PubMed](#)]
24. Zhu, M.; Tang, J.; Tu, X.; Chen, W. Determination of Ascorbic Acid, Total Ascorbic Acid, and Dehydroascorbic Acid in Bee Pollen Using Hydrophilic Interaction Liquid Chromatography-Ultraviolet Detection. *Molecules.* **2020**, *25*, 5696. [[CrossRef](#)] [[PubMed](#)]
25. Chang, J.; Lv, W.; Li, Q.; Li, H.; Li, F. One-Step Synthesis of Methylene Blue-Encapsulated Zeolitic Imidazolate Framework for Dual-Signal Fluorescent and Homogeneous Electrochemical Biosensing. *Anal. Chem.* **2020**, *92*, 8959–8964. [[CrossRef](#)] [[PubMed](#)]
26. Wu, J.; Lv, W.; Yang, Q.; Li, H.; Li, F. Label-free homogeneous electrochemical detection of MicroRNA based on target-induced anti-shielding against the catalytic activity of two-dimension nanozyme. *Biosens. Bioelectron.* **2021**, *171*, 112707. [[CrossRef](#)] [[PubMed](#)]
27. Antoniazzi, C.; Lima, C.; Marangoni, R.; Castro, E.; Santana, E.; Spinelli, A. Molybdenum trioxide incorporated in a carbon paste as a sensitive device for bisphenol A monitoring. *Microchem. J.* **2020**, *159*, 105528. [[CrossRef](#)]
28. Wu, J.; Yang, Q.; Li, Q.; Li, H.; Li, F. Two-Dimensional MnO₂ Nanozyme-Mediated Homogeneous Electrochemical Detection of Organophosphate Pesticides without the Interference of H₂O₂ and Color. *Anal. Chem.* **2021**, *93*, 4084–4091. [[CrossRef](#)]
29. Dhara, K.; Debiprosad, R.M. Review on nanomaterials-enabled electrochemical sensors for ascorbic acid detection. *Anal. Biochem.* **2019**, *586*, 113415. [[CrossRef](#)]
30. Savk, A.; Ozdil, B.; Demirkan, B.; Nas, M.S.; Calimli, M.H.; Alma, M.H.; Inamuddin; Asiri, A.M.; Sen, F. Multiwalled carbon nanotube-based nanosensor for ultrasensitive detection of uric acid, dopamine, and ascorbic acid. *Mater. Sci. Eng. C-Mater. Biol. Appl.* **2019**, *99*, 248–254. [[CrossRef](#)]

31. Xu, C.; Liu, B.; Ning, W.; Wang, X. Highly Sensitive Ascorbic Acid Sensor Based on Ionic Liquid Functionalized Graphene Oxide Nanocomposite. *Int. J. Electrochem. Sci.* **2019**, *14*, 1670–1683. [[CrossRef](#)]
32. Jiang, Y.; Xiao, X.; Li, C.; Luo, Y.; Chen, S.; Shi, G.; Han, K.; Gu, H. Facile Ratiometric Electrochemical Sensor for In Vivo/Online Repetitive Measurements of Cerebral Ascorbic Acid in Brain Microdialysate. *Anal. Chem.* **2020**, *92*, 3981–3989. [[CrossRef](#)] [[PubMed](#)]
33. Wang, L.; Xie, Y.; Yang, Y.; Liang, H.; Wang, L.; Song, Y. Electroactive Covalent Organic Frameworks/Carbon Nanotubes Composites for Electrochemical Sensing. *ACS Appl. Nano Mater.* **2020**, *3*, 1412–1419. [[CrossRef](#)]
34. Ma, Y.; Zhang, Y.; Wang, L. An electrochemical sensor based on the modification of platinum nanoparticles and ZIF-8 membrane for the detection of ascorbic acid. *Talanta* **2021**, *226*, 122105. [[CrossRef](#)]
35. Ben Hassine, A.; Raouafi, N.; Moreira, F.T.C. Novel Electrochemical Molecularly Imprinted Polymer-Based Biosensor for Tau Protein Detection. *Chemosensors* **2021**, *9*, 238. [[CrossRef](#)]
36. Leibl, N.; Haupt, K.; Gonzato, C.; Duma, L. Molecularly Imprinted Polymers for Chemical Sensing: A Tutorial Review. *Chemosensors* **2021**, *9*, 123. [[CrossRef](#)]
37. Qiu, Z.; Fan, D.; Xue, X.; Guo, S.; Lin, Y.; Chen, Y.; Tang, D. Molecularly Imprinted Polymer Functionalized Bi₂S₃/Ti₃C₂TX MXene Nanocomposites for Photoelectrochemical/Electrochemical Dual-Mode Sensing of Chlorogenic Acid. *Chemosensors* **2022**, *10*, 252. [[CrossRef](#)]
38. Cui, F.; Zhou, Z.; Zhou, H.S. Molecularly Imprinted Polymers and Surface Imprinted Polymers Based Electrochemical Biosensor for Infectious Diseases. *Sensors* **2020**, *20*, 996. [[CrossRef](#)]
39. Singhal, A.; Parihar, A.; Kumar, N.; Khan, R. High throughput molecularly imprinted polymers based electrochemical nanosensors for point-of-care diagnostics of COVID-19. *Mater. Lett.* **2022**, *306*, 130898. [[CrossRef](#)]
40. Wang, B.; Hong, J.; Liu, C.; Zhu, L.; Jiang, L. An Electrochemical Molecularly Imprinted Polymer Sensor for Rapid beta-Lactoglobulin Detection. *Sensors* **2021**, *21*, 8240. [[CrossRef](#)]
41. Asif, M.H.; Razaq, A.; Akbar, N.; Danielsson, B.; Sultana, I. Facile synthesis of multisegment Au/Ni/Au nanowire for high performance electrochemical glucose sensor. *Mater. Res. Express* **2019**, *6*, 095028. [[CrossRef](#)]
42. Cai, Y.; Zhu, H.; Zhou, W.; Qiu, Z.; Chen, C.; Qileng, A.; Li, K.; Liu, Y. Capsulation of AuNCs with AIE Effect into Metal-Organic Framework for the Marriage of a Fluorescence and Colorimetric Biosensor to Detect Organophosphorus Pesticides. *Anal. Chem.* **2021**, *93*, 7275–7282. [[CrossRef](#)]
43. Xiao, T.; Huang, J.; Wang, D.; Meng, T.; Yang, X. Au and Au-Based nanomaterials: Synthesis and recent progress in electrochemical sensor applications. *Talanta* **2020**, *206*, 120210. [[CrossRef](#)] [[PubMed](#)]
44. Guo, Y.; Wang, L.; Xu, L.; Peng, C.; Song, Y. A ascorbic acid-imprinted poly(o-phenylenediamine)/zeolite imidazole frameworks-67/carbon cloth for electrochemical sensing ascorbic acid. *J. Mater. Sci.* **2020**, *55*, 9425–9435. [[CrossRef](#)]
45. Fu, M.; Xu, F.; Yan, J.; Wang, C.; Fan, G.; Song, G.; Chai, B. Mixed valence state cerium metal organic framework with prominent oxidase-mimicking activity for ascorbic acid detection: Mechanism and performance. *Colloids Surf. A-Physicochem. Eng. Asp.* **2022**, *641*, 128610. [[CrossRef](#)]
46. Wang, L.; Pan, L.; Han, X.; Ha, M.N.; Li, K.; Yu, H.; Zhang, Q.; Li, Y.; Hou, C.; Wang, H. A portable ascorbic acid in sweat analysis system based on highly crystalline conductive nickel-based metal-organic framework (Ni-MOF). *J. Colloid Interface Sci.* **2022**, *616*, 326–337. [[CrossRef](#)]
47. Ma, T.; Meng, J.; Song, Q.; Wen, D. Superhydrophilic edge-rich graphene for the simultaneous and disposable sensing of dopamine, ascorbic acid, and uric acid. *J. Mater. Chem. B* **2022**, *10*, 1094–1102. [[CrossRef](#)]
48. Xi, X.; Wu, D.; Ji, W.; Zhang, S.; Tang, W.; Su, Y.; Guo, X.; Liu, R. Manipulating the Selectivity of OECT-Based Biosensors via the Surface Engineering of Carbon Cloth Gate Electrodes. *Adv. Funct. Mater.* **2020**, *30*, 1905361. [[CrossRef](#)]
49. Franco, F.d.S.; Fernandes, D.S.; Do Carmo, D.R. A modified hybrid silsesquioxane/histidine composite for copper and zinc adsorption and its behavior in the electro-oxidation of ascorbic acid. *Mater. Sci. Eng. C-Mater. Biol. Appl.* **2020**, *111*, 110739. [[CrossRef](#)]
50. Cai, X.; Wei, C.; Dong, J.; Liu, Q.; Wu, Y.; Lu, G.; Chen, Y.; Jiang, J. Dimeric phthalocyanine-involved double-decker complex-based electrochemical sensor for simultaneous detection of acetaminophen and ascorbic acid. *J. Mater. Sci.—Mater. Electron.* **2019**, *30*, 1976–1983. [[CrossRef](#)]
51. Mazzara, F.; Patella, B.; Aiello, G.; O’Riordan, A.; Torino, C.; Vilasi, A.; Inguanta, R. Electrochemical detection of uric acid and ascorbic acid using r-GO/NPs based sensors. *Electrochim. Acta* **2021**, *388*, 138652. [[CrossRef](#)]
52. Rossato, J.H.H.; Oliveira, M.E.; Lopes, B.V.; Gallo, B.B.; La Rosa, A.B.; Piva, E.; Barba, D.; Rosei, F.; Carreño, N.L.V.; Escote, M.T. A Flexible Electrochemical Biosensor Based on NdNiO₃ Nanotubes for Ascorbic Acid Detection. *ACS Appl. Nano Mater.* **2022**, *5*, 3394–3405. [[CrossRef](#)]
53. Ibarlucea, B.; Roig, A.P.; Belyaev, D.; Baraban, L.; Cuniberti, G. Electrochemical detection of ascorbic acid in artificial sweat using a flexible alginate/CuO-modified electrode. *Microchim. Acta* **2020**, *187*, 520. [[CrossRef](#)] [[PubMed](#)]